J. Fluid Mech. (1994), *vol.* 279, *pp.* 217–237

A numerical study of the vorticity field generated by the baroclinic effect due to the propagation of a planar pressure wave through a cylindrical premixed laminar flame

By G. A. BATLEY[1,2], A. C. McINTOSH[1], J. BRINDLEY[2] AND S. A. E. G. FALLE[2]

[1] Department of Fuel and Energy, Leeds University, Leeds LS2 9JT, UK

[2] Department of Applied Mathematics, Leeds University, Leeds LS2 9JT, UK

(Received 12 November 1993 and in revised form 22 June 1994)

The importance of vorticity production in combustion systems has been highlighted previously by several authors (Markstein 1964; Picone *et al.* 1984). The consequent distortion and enlargement of flame surfaces can lead to substantial enhancement of the burning rate which may be beneficial or disastrous depending on the physical context. We describe the results of numerical simulations of an experimental configuration similar to that described by Scarinci & Thomas (1992), who examined the effect of initially planar pressure signals on two-dimensional flame balls. The flame ball is here set-up from ignition using a code, based on the second-order Godunov scheme described by Falle (1991). A simple Arrhenius reaction scheme is adopted in modelling a unimolecular decomposition. As in previous papers (Batley *et al.* 1993*a*, *b*) the thermal conductivity is assumed to vary linearly with temperature, and the Lewis and Prandtl numbers are taken as unity. A short time after ignition, when the flame ball has reached a radius of approximately 2 cm, a very short-lengthscale pressure step disturbance is introduced, propagating towards the combustion region. As the signal crosses the flame, the interaction of the sharp, misaligned pressure and density gradients, creates a strong vorticity field. The resulting roll-up of the flame eventually divides it into two smaller rotating reacting regions. In order to gauge the effect of the chemical reaction and in particular the viscous diffusion on the evolution of the vorticity field, the results are compared with analogous solutions of the Euler equations.

1. Introduction

The importance of the baroclinic effect in combustion systems has been highlighted previously in both experimental and computational studies. Markstein (1964) described an experiment involving the interaction of an initially planar shock with a spherical flame bubble in a shock tube which was closed at one end. The photographs of this interaction showed clearly the onset of rotational gaseous motion induced by the first passage of the shock. As the subsequent reflected disturbance crossed the flame, increasing the strength of the vorticity field, smaller-scale eddies were produced, which eventually lead to the turbulent breakup of the flame and so to a massive increase in the overall burning rate. Using both numerical and analytical techniques, Picone *et al.* (1984) studied a similar experimental set-up involving the interaction of a planar shock

with a cylindrically symmetric flame ball. By modelling the flame ball as a region of density inhomogeneity with a prescribed spatial profile, these authors were able to derive an approximate analytical expression for the strength of the two vortices produced by the first passage of the shock by ignoring variations in the shock strength and geometry. They then used a code, based on FAST2D, described by Book *et al.* (1981), to solve the Euler equations, and were able to reproduce accurate representations of the early part of the interaction, dominated by gasdynamic effects.

In this paper, a single passage of an ultra-short-lengthscale pressure step across an expanding flame front is considered (cf. Scarinci & Thomas 1992). A second-order Godunov scheme is used to solve the equations governing the behaviour of a reacting fluid with unit Lewis and Schmidt numbers. The code used is based on that described by Falle (1991). A unimolecular decomposition reaction whose rate has an Arrhenius temperature dependence is considered, and the thermal conductivity is assumed to be proportional to temperature.

The first aim of the numerical study is to model the ignition of the gas via a slow deposition of energy within a small cylindrical region. Using a simplified version of the code, designed for cylindrical symmetry, the energy input required for initiation is calculated, and the propagation of the laminar flame is modelled using a minimum of computing time. The data describing the state of the flame at a given time after ignition, generated by the one-dimensional code, is then interpolated into a two-dimensional Cartesian grid. A propagating pressure disturbance with fractional amplitude 0.3 compared to ambient, and lengthscale 4 mm is set up at a sufficient distance from the flame ball for the initial evolution of both to be considered mutually independent. Initially, this pressure disturbance therefore propagates uniformly towards the flame ball. As the signal traverses the flame region, the baroclinic effect, due to the misalignment of the pressure gradient with the density gradient associated with the flame, produces a significant vorticity field. This vorticity field causes the flame front to curl in on itself in a manner similar to that of the behaviour of the cylindrical vortex sheets examined by Rottman & Stansby (1993).

In order to gauge the importance of the reaction and diffusion processes, the results are compared with the evolution of the same density inhomogeneity after the passage of the same pressure disturbance, with (i) the reaction term set to zero and (ii) both the reaction and diffusion (thermal, species and viscous) terms set to zero. (Note that the particular importance of viscosity in determining the behaviour of strong vorticity fields has been highlighted previously by several authors, including Cloutman & Wehner 1992 and Rottman & Stansby 1993.)

A relatively weakly reaction mixture is assumed, giving a slow laminar flame speed and a broad reaction zone (≈ 4 mm). Because the Mach number of the flame is so low (of the order 10^{-4}), the time taken for the pressure disturbance to traverse the preheat zone, and in fact the entire flame ball, is far too short for the combustion processes to contribute significantly to the flow during this stage of the interaction, unless temperature increases associated with the pressure signal are sufficient to cause exponential burning rate changes (cf. McIntosh 1989, 1991, 1993; McIntosh, Batley & Brindley 1993). The latter of these two papers, together with the follow up work, Batley, McIntosh & Brindley (1993*a*), describes detailed numerical investigations into interactions between short-lengthscale planar pressure signals with planar flames in one space dimension. In particular, the effect of the flame's density distribution on the pressure signal is examined in detail and it is demonstrated that the amplitude increases if the signal approaches from the equilibrium side, and decreases if it approaches from the preheat side. It is further described in Batley *et al.* (1993*a*) that the flame undergoes

a sharp burning rate increase after a positive pressure step before diffusing back to a new steady state. However, for the fractional increase in pressure in the current work (0.3), the effects of this increase in burning rate, as well as those of the differential convection of the flame with the disturbance, are quite small, and can be neglected in order to provide a simple mathematical model of the interaction. A coarse approximation to the contribution of the baroclinic effect can be made by further neglecting the variation in the strength and geometry of the incident signal.

An approximate form for the vorticity field generated by the interaction can then be found, simply by imposing the uniformly propagating pressure signal on the density field of the flame. This approach has been used previously by Scarinci (1990), who derived expressions for the total circulation generated by the interaction of a planar shock with both a cylindrical and a spherical flame ball. After the initial interaction, the cylindrical flame front can reasonably be modelled as a thin annulus on which the vortex strength varies sinusoidally. This set-up has been examined previously by Krasny (1986*b*) as a model of the inviscid motion of a cylinder of fluid released from rest in a cross-flow. In that paper, the author succeeded in solving numerically the equations of motion for such a vortex sheet. However, the solutions presented were only valid over very short times leading up to the formation of a pair of singularities. There has recently been greater success in solving the simplified equations derived for the case where the gases on either side of the vortex sheet have the same density (see for example Rottman, Simpson & Stansby 1987; Rottman & Stansby 1993). The results presented here confirm that the initial behaviour of the cylindrical vortex sheet separating gases with differing densities is qualitatively similar to that in the case where the gases have the same density.

The major difference between the current study and both the vortex sheet studies described above and the theoretical and numerical studies of the evolution of vorticity fields in combustion systems, is that here the effects of the chemical reaction and of thermal and mass diffusion are included. Although the reactivity of the mixture considered here is very low, it is demonstrated that, within a few milliseconds of the initial interaction, the combustion processes begin to cause the disintegration of the small-scale coiled reaction front structure.

2. Governing equations

The two-dimensional reactive Navier–Stokes equations are solved in terms of the vector of conserved variables U given by

$$U = \begin{pmatrix} \rho \\ \rho u_x \\ \rho u_y \\ e \\ \rho C \end{pmatrix}, \tag{2.1}$$

where ρ is the gas density, $\boldsymbol{u} = (u_x, u_y)$ the gas velocity vector, e the total kinetic and thermal energy per unit volume and C the fuel mass fraction. The full set of governing equations is then given by

$$\frac{\partial \boldsymbol{U}}{\partial t} + \frac{\partial (\boldsymbol{F}_x + \boldsymbol{F}_{Dx})}{\partial x} + \frac{\partial (\boldsymbol{F}_y + \boldsymbol{F}_{Dy})}{\partial y} = \boldsymbol{S}, \tag{2.2}$$

where $\boldsymbol{F}_x$ and $\boldsymbol{F}_y$ are the usual hyperbolic flux vectors given by

$$\boldsymbol{F}_x = \begin{pmatrix} \rho u_x \\ p + \rho u_x^2 \\ \rho u_x u_y \\ u_x(e+p) \\ \rho u_x C \end{pmatrix} \tag{2.3}$$

and

$$\boldsymbol{F}_y = \begin{pmatrix} \rho u_y \\ \rho u_x u_y \\ p + \rho u_y^2 \\ u_y(e+p) \\ \rho u_y C \end{pmatrix}, \tag{2.4}$$

$\boldsymbol{F}_{Dx}$ and $\boldsymbol{F}_{Dy}$ are the diffusive flux vectors

$$\boldsymbol{F}_{Dx} = \begin{pmatrix} 0 \\ -\tau_{xx} \\ -\tau_{xy} \\ -\lambda \dfrac{\partial T}{\partial x} - u_x \tau_{xx} - u_y \tau_{xy} \\ -D\rho\, \partial C/\partial x \end{pmatrix} \tag{2.5}$$

and

$$\boldsymbol{F}_{Dy} = \begin{pmatrix} 0 \\ -\tau_{yx} \\ -\tau_{yy} \\ -\lambda \dfrac{\partial T}{\partial y} - u_y \tau_{yy} - u_x \tau_{yx} \\ -D\rho\, \partial C/\partial y \end{pmatrix}, \tag{2.6}$$

$\boldsymbol{\tau}$ being the usual stress tensor

$$\boldsymbol{\tau} = \mu \begin{pmatrix} \dfrac{4}{3}\dfrac{\partial u_x}{\partial x} - \dfrac{2}{3}\dfrac{\partial u_y}{\partial y} & \dfrac{\partial u_x}{\partial y} + \dfrac{\partial u_y}{\partial x} \\ \dfrac{\partial u_x}{\partial y} + \dfrac{\partial u_y}{\partial x} & \dfrac{4}{3}\dfrac{\partial u_y}{\partial y} - \dfrac{2}{3}\dfrac{\partial u_x}{\partial x} \end{pmatrix}, \tag{2.7}$$

and the source vector $\boldsymbol{S}$ includes the contribution of the chemical reaction to the energy and species distributions. $\boldsymbol{S}$ may be written

$$\boldsymbol{S} = \begin{pmatrix} 0 \\ 0 \\ 0 \\ Q\rho C\, \mathrm{e}^{-E_A/\Re T} \\ -\rho C\, \mathrm{e}^{-E_A/\Re T} \end{pmatrix}. \tag{2.8}$$

In (2.3)–(2.8) p is the gas pressure, λ the thermal conductivity, D the relative species diffusion coefficient, μ the coefficient of dynamic viscosity, Q the specific heat release, E_A the release activation energy, $\Re$ is the gas constant, and T the gas temperature.

In this work it is assumed that

$$\lambda \propto T, \tag{2.9}$$

and that the Lewis and Prandtl numbers, defining the relative importance of thermal, mass and viscous diffusion, are both equal to unity.

3. Numerical scheme

The code used for this work is second-order accurate in both space and time. The Godunov scheme employed divides the (x, y)-plane into grid cells with the variable values calculated at the cell centroids. A nonlinear Riemann solver is then used to calculate the hyperbolic fluxes at the cell boundaries. The first-order time step takes the distributions within each cell to be uniform. The second-order time step then gives second-order space accuracy by using adjacent mid-cell values to calculate the flow-quantity gradients. In order to maintain monotonicity, an averaging function is employed in the regions with large second derivatives to reduce the accuracy of the scheme to first order. Diffusive fluxes are then also calculated at the cell boundaries and the reaction terms evaluated using cell-centroid values. The details of the hyperbolic part of the numerical scheme are described by Falle (1991) for cylindrical geometry.

The flame is initiated by a slow energy input within a small cylindrical region with radius 1.5 mm. It is assumed that ignition takes place a sufficient distance from any solid boundary for reflected pressure signals to be insignificant. This assumption allows the use of a one-dimensional scheme, designed for cylindrical symmetry, in examining the ignition phase of this simulation. There are obvious practical advantages in being able to set up the propagating flame ball in one space dimension. Clearly the CPU time required for integrations at the same resolution is minimal in one dimension compared with two, and this is particularly important since the ignition phase can take up to 0.05–0.1 s. However, setting up the propagating cylindrical flame requires higher resolution in two dimensions than in one. This is because in two Cartesian dimensions a small number of data points within the ignition region results in a propagating flame whose structure is grid dependent, in that the reaction zone tends to become square as the resolution is decreased. If, to overcome this problem, the energy is deposited within a larger region, the reduction in thermal diffusion means that the central temperature reaches much higher values once the reaction has begun, and takes much longer to diffuse back to the adiabatic burnt gas temperature. Because of the Arrhenius reaction term, these high temperatures mean that an exceedingly short time step is required in order to maintain accuracy, and in particular to avoid the unphysical occurrence of a locally negative fuel mass fraction. Thus modelling the ignition phase in two space dimensions would require a massive amount of computing time, and the one-dimensional scheme is therefore used for this part of the simulation.

The spatial and temporal resolution required is determined by the need to capture the various important physical processes.

3.1. *Spatial resolution*

The spatial resolution used in the simulations is determined by the need to resolve the sharply peaked Arrhenius reaction term, whose contribution to the energy and species equations must be calculated accurately. Here the grid size is chosen so that there are roughly 10 data points within the 90 % reaction rate thickness of the propagating flame ball. Steady planar flame characteristics are taken as a rough guide to the thickness of the cylindrical flame. (Note that as the radius of the propagating flame increases, curvature effects become less significant, and the planar approximation becomes more accurate.)

The combusion parameters chosen for this work are given by:

unburnt gas temperature:

$$T_u = 300 \text{ K}, \tag{3.1}$$

burnt gas temperature:

$$T_b = 1500 \text{ K}, \tag{3.2}$$

ratio of T_u to T_b:

$$T_{01} = 0.2, \tag{3.3}$$

dimensionless activation energy $E_A/\Re T_b$:

$$\theta = 10, \tag{3.4}$$

reaction rate constant:

$$k_s = 5 \times 10^7 \text{ s}^{-1}, \tag{3.5}$$

Lewis number:

$$D_u \rho_u c_p / \lambda_u = 1, \tag{3.6}$$

Schmidt number:

$$\mu_u / \rho_u D_u = 1, \tag{3.7}$$

thermal diffusion coefficient:

$$\lambda_u = 0.1 \text{ J m}^{-1} \text{ s}^{-1} \text{ K}^{-1}, \tag{3.8}$$

density:

$$\rho_u = 1.17 \text{ kg m}^{-3}, \tag{3.9}$$

and therefore

$$\frac{\lambda_u}{\rho_u c_p} = 9 \times 10^{-5} \text{ m}^2 \text{ s}^{-1}. \tag{3.10}$$

The subscripts u and b refer to unburnt and burnt values, respectively, and c_p is the specific heat capacity. For this set of values, for a steadily propagating planar flame involving a single unimolecular decomposition reaction with thermal conductivity proportional to temperature and Lewis number equal to unity, high-activation-energy asymptotic analysis yields a flame speed of 7.75 cm s^{-1} and a 90% reaction zone thickness of about 4 mm. (See for example Clarke & McIntosh 1984 for a description of the planar flame model.) Thus in this work the grid size used is 0.4 mm.

Of course, the spatial resolution used also plays an important role in the rest of the simulation. As mentioned earlier, the ignition region has a spatial scale of 1.5 mm. Although the number of grid points within this region is very small, use of the one-dimensional code means that this number is sufficient, since precise analysis of ignition is not the focus of interest here. The crucial phase of the simulation is the evolution of the flame ball after the passage of the pressure signal. As indicated by previous studies of the roll-up of cylindrical vortex sheets (e.g. Rottman & Stansby 1993), the rate of progression towards small-scale structures depends on the amount of viscosity. In this paper, comparisons are made between solutions of the equations with and without viscosity, and the point at which the grid becomes inadequate is clearly shown in the latter case.

(Consideration must also be given to the thickness of the initial boundary layer. Taking the radius of the flame ball and the gas velocity behind the pressure disturbance as typical flow values gives a Reynolds number of the order 10^3–10^4. The initial viscous boundary-layer thickness, which is proportional to $Re^{-1/2}$, is therefore of the order of 0.1 mm, and so cannot be fully resolved using the current grid size of 0.4 mm. However, comparison of results with analogous early-time solutions of the Euler equations indicate that prediction of the behaviour of the flame front is at least qualitatively correct.)

3.2. *Temporal resolution*

As described by Falle (1991), the stability of the hyperbolic part of the numerical scheme requires a time step (Δt) which obeys the usual Courant restriction

$$\Delta t < \frac{\Delta x}{(a + |\boldsymbol{u}|)_{max}}, \tag{3.11}$$

where $\boldsymbol{u}$ is the velocity vector and a is the local sound speed. In this work the Courant number is set equal to 0.4, which leads to time steps of the order 10^{-7} s; this is a much tighter restriction than that imposed by the diffusion terms. However, in order to maintain accuracy, and in particular to avoid the occurrence of negative values of C (the fuel mass fraction), an extra restriction is imposed on the size of the time step. This condition is given by

$$\Delta t < \frac{\epsilon}{k_s \mathrm{e}^{-E_A/\Re T_{max}}}, \tag{3.12}$$

where ϵ is a positive number which is less than unity, giving the maximum allowable fractional change in fuel concentration due to the chemical reaction within a single time step. In the simulations described here, the value of ϵ is set to 0.2.

4. Ignition

The cylindrical flame is initiated by a slow energy input within a small central region with radius of the order of 1.5 mm. The time taken for the energy to be deposited is much longer than the timescale typifying the passage of an acoustic signal across the ignition region. Thus the vast majority of the deposited energy is carried out of the central regions in the form of kinetic energy such that the reactants flow radially outward, driven by a small but significant pressure gradient. This outflow of gas leads to decreasing density within the ignition region, and thus, with the pressure effectively constant, the overall effect is that the temperature increases inversely with the density. It is possible to obtain an approximate value for the central temperature achieved for a given energy input by neglecting thermal and viscous diffusion effects. Without these terms the energy equation can be written

$$\frac{\mathrm{D}\ln T}{\mathrm{D}t} = \frac{(\gamma-1)}{\gamma}\frac{\mathrm{D}\ln p}{\mathrm{D}t} + \frac{(\gamma-1)S(r,t)}{p}, \tag{4.1}$$

where

$$\frac{\mathrm{D}}{\mathrm{D}t} = \frac{\partial}{\partial t} + \boldsymbol{u}\cdot\boldsymbol{\nabla}, \tag{4.2}$$

$S(r,t)$ is the rate of energy input, and γ the ratio of specific heats.

If pressure variations are assumed negligible, then the temperature at the origin, where $\boldsymbol{u} \equiv \boldsymbol{0}$, is simply given by

$$T(0,t) = T(0,0)\exp\left(\int_0^t \frac{(\gamma-1)S(0,t'')}{p}\mathrm{d}t''\right). \tag{4.3}$$

The energy is assumed to be deposited in a small expanding cylindrical region at a rate which increases to a peak and then dies away with time. The exact form of the source term is given by

$$S(r,t) = A(t)\mathrm{e}^{-k_r(t)r^2}, \tag{4.4}$$

where

$$A(t) = A_0\mathrm{e}^{-k_t(t-t_p)^2}, \tag{4.5}$$

and

$$k_r(t) = k_{r0}(1+\alpha t_p/(t+t_p)). \tag{4.6}$$

(Thus the approach is similar to that described by Oran & Boris 1979.) Here t_p is the time of maximum power input, and α defines the evolution of the spatial scale of the energy input region. If $\mathrm{e}^{-kt_p^2}$ is small, it follows that

$$T(0,t\to\infty) = T(0,0)\exp\left(\frac{A_0(\gamma-1)}{pk_t^{1/2}}\right). \tag{4.7}$$

Since ignition requires a temperature increase by a factor $1/T_{01}$, the value of A_0 required is

$$\frac{\ln(1/T_{01})pk_t^{1/2}}{(\gamma-1)}.$$

In reality, diffusive losses mean that the final temperature achieved will be significantly lower than the above analysis would indicate, but the time taken for the one-dimensional code to run is very low, making calculation of a suitable value for A_0 using the above value as a first guess a simple matter.

5. Two-dimensional interaction

The one-dimensional ignition code is allowed to run until the central temperature peak has died away, so that the temperature of the burnt gas is approximately uniform and the flame has reached the required radius. The data is then read into a two-dimensional Cartesian grid to be used as the initial condition for the pressure interaction. In order to maintain second-order accuracy, the distance between the centroids of corresponding Cartesian and cylindrical grid cells is taken into account. A planar pressure disturbance is next introduced, propagating towards the flame ball in the unburnt region. This disturbance is set up by choosing the associated velocity distribution so that the Riemann variable corresponding to the direction opposite to that of the propagation of the disturbance is unchanged (see for example Crighton 1986 or Whitham 1974). Hence a pressure step function of the form

$$p(x,y) = p_u(1+\beta H(y-y_0)\{1-\operatorname{sech}^2[k(y-y_0)]\}), \tag{5.1}$$

is introduced, with an associated adiabatic density field given by

$$\rho(x,y) = \rho_u(1+\beta H(y-y_0)\{1-\operatorname{sech}^2[k(y-y_0)]\})^{1/\gamma}, \tag{5.2}$$

and a velocity perturbation given by

$$u_y = \frac{-2}{(\gamma-1)}\left[\left(\frac{\gamma p(x,y)}{\rho(x,y)}\right)^{1/2} - \left(\frac{\gamma p_u}{\rho_u}\right)^{1/2}\right]. \tag{5.3}$$

Note that, in the above set, β defines the fractional amplitude of the pressure signal, which in this paper is equal to 0.3. In order to reduce the required spatial domain of integration, the frame of reference chosen for the two-dimensional grid moves at uniform velocity with the gas behind the pressure disturbance.

6. Results and discussion

6.1. *Ignition*

Figure 1 shows the evolution of the temperature and fuel mass fraction at the centre of the external energy input for various amplitudes (A_0). The numbered lines show the results for increasing amplitudes of energy input. The first amplitude is chosen so that the central temperature would reach a value just less than the adiabatic burnt gas temperature of the steady flame in the absence of diffusive and acoustic heat losses. The amplitude is then increased by one twentieth of this value for successive integrations. The central temperature estimates for each amplitude are given in the figure.

(Note that the ambient gas temperature (T_u) is 300 K, and $T_{01} = 0.2$ which gives $T_b = 1500$ K.) The values of the other parameters describing the energy input, which

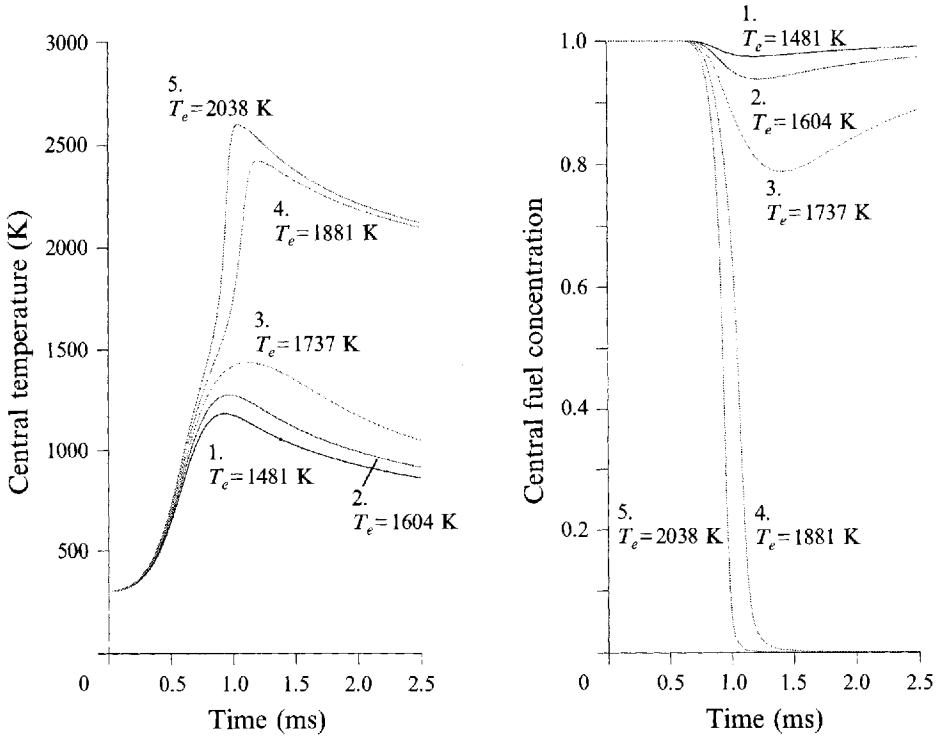

FIGURE 1. The evolution of the central temperature and fuel concentration during various slow energy inputs. Curve 1: $A_0 = 4200$ J m^{-3} s^{-1}; 2, $A_0 = 4410$ J m^{-3} s^{-1}; 3, $A_0 = 4620$ J m^{-3} s^{-1}; 4, $A_0 = 4830$ J m^{-3} s^{-1}; 5, $A_0 = 5040$ J m^{-3} s^{-1}.

determine the importance of diffusive and acoustic losses, and the time taken for the flame to settle down after ignition, are given by

$$\alpha = 0.2,$$

$$t_p = 5 \times 10^{-4} \text{ s},$$

$$\text{time half-thickness } (= (\ln(2)/k_t)^{1/2}) = 2.5 \times 10^{-4} \text{ s},$$

and

$$\text{final radial half-thickness } (= (\ln(2)/k_{r0})^{1/2}) = 1.5 \text{ mm}.$$

Pressure fluctuations induced by energy inputs at the rates determined by this set of parameters are limited to fractional amplitudes of the order of 10^{-3} of ambient, so that the energy losses associated with propagating acoustic waves are small. The major heat loss during ignition is therefore due to thermal diffusion. Figure 2 shows the flame at a time 0.085 s after ignition with ignition characteristics corresponding to line 4. By this time the central temperature peak has died away, and since the radius of the flame is now 2 cm, which is quite large compared with the flame thickness, curvature effects on the flame structure are small.

6.2. *Pressure–flame interaction*

6.2.1. *Comparison of early stages with vortex-sheet evolution*

The evolution of the density, vorticity, fuel mass fraction and reaction rate distributions during the early stages of the interaction are shown in figures 3 and 4. Successive time plots are shown at 0.25 ms intervals. (Note that in figures 3 and 4 as

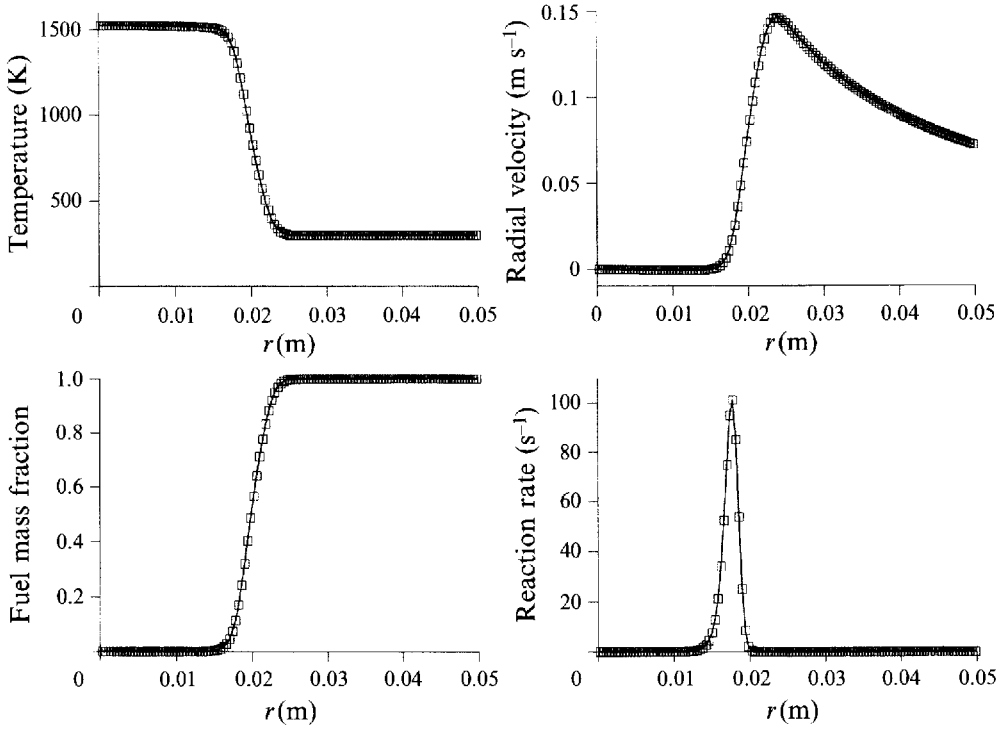

FIGURE 2. The temperature, radial velocity, fuel mass fraction and reaction rate distributions within the flame, 0.085 s after initiation.

well as figures 6 and 7, the range of values covered by the associated scale is determined by the range of values present within each plot.) Figures 3(*a*)–3(*d*) show the full extent of the integration domain. The initial location of the flame ball is shown clearly in the density, fuel mass fraction and reaction rate plots (the left-hand plots of figures 3(*a*)–3(*d*) respectively). The initial density distribution also shows the location of the imposed pressure signal within the unburnt region above the flame.

In the central plots of figures 3(*a*)–3(*d*) ($t = 0.08525$ s), the flame ball has moved slightly in the direction opposite to that of the pressure signal propagation. This is because, in order to reduce the size of the spatial domain modelled, the frame of reference is moving in the same direction as the shock, at the initial speed of the gas immediately behind it. These latter plots of the early part of the interaction also show a slight deformation of the flame by the time the pressure signal has passed through the combustion region. The increase in reaction rate shown in the second plot of figure 3(*d*) is due to the adiabatic temperature rise associated with the pressure step, and the resultant narrowing of the reaction zone at the front end of the flame ball has been previously commented on by Batley (1993) and Batley, McIntosh & Brindley (1993*a*, *b*).

A significant annular vorticity field is seen to have been induced within the flame by the baroclinic impulse (central plot of figure 3*b*). The continuing evolution, which is governed largely by this vorticity field, shows that within 1 ms of the start of the interaction ($t = 0.086$ s, shown in the top central plots of figures 4(*a*)–4(*d*)), the rotational velocity field has drawn the cold unburnt gas from the region immediately above the flame right through the combustion region, splitting it into two distinct components. Within each of these components, the thick vorticity sheet continues to

roll up, and after another millisecond ($t = 0.087$ s, shown in the bottom right hand plots of figures 4(*a*)–4(*d*)) a spiral structure, similar to that found by Rottman & Stansby (1993), is apparent. The behaviour of the reaction zone (figure 4(*d*)) broadly follows the behaviour of the vortex sheet (figure 4*b*), continuing to coil in on itself, thus mixing the cold unburnt fuel from outside the original flame ball with the hot burnt gas within.

Using a simple model which includes only the dominant physical effects, a rough analytical form for the initial vorticity field can be derived. In this calculation, the following approximations are included:

(i) The time taken for the pressure signal to traverse the flame region is assumed to be sufficiently short for the radial propagation of the flame front during this time to be neglected.

(ii) Variations in the amplitude and geometry of the pressure signal are neglected.

(iii) Distortion of the flame due to differential convection with the flow behind the pressure signal is neglected, so that the flame is treated as if its entire structure is given a uniform and instantaneous linear impulse and is therefore initially uniformly convected at the initial speed of the gas behind the pressure signal.

(It is also assumed that the passage of the pressure signal is sufficiently rapid for the baroclinic impulse over the entire flame region to be considered instantaneous.)

The flame can then be modelled as a cylindrically symmetric density distribution which instantaneously undergoes simultaneous linear and baroclinic impulses. By then following the approach of Scarinci (1990), and integrating the baroclinic term $\nabla(1/\rho)\times\nabla p$, it can be shown that the total circulation generated (Γ_0) is equal to

$$\Gamma_0 = \frac{2r_0 c_0}{\gamma}\left(\frac{p^+}{p^-}-1\right)\left(1-\frac{\rho_u}{\rho_b}\right), \tag{6.1}$$

with the circulation strength per unit azimuthal angle ($V(\eta)$) being equal to

$$V(\eta) = r_0\left(\frac{p^+-p^-}{c_0\rho_u}\right)\left(1-\frac{1}{T_{01}}\right)\sin\eta, \tag{6.2}$$

where η is the acute angle between the position vector $\boldsymbol{r}$ and the y-axis, the direction of which is taken to be opposite to that of the motion of the pressure signal. Here p^+ and p^- are the gas pressures behind and ahead of the imposed disturbance, and c_0 is the speed of sound in the unburnt gas.

The evolution of vortex sheets embedded in ideal flows has received much attention in recent years. In particular, a large number of papers have described numerical techniques based on the point-vortex method, originally suggested by Rosenhead (1931). By modelling an inviscid sheet as a collection of point vortices, Rosenhead was able to derive an evolution equation for the locus of these points on the basis of constant vortex strength. However, as described by, amongst others, Rottman *et al.* (1987), this technique suffers from fundamental difficulties arising from the susceptibility of these systems to short-lengthscale Helmholtz instabilities. A more fundamental problem is that these inviscid models predict the formation of a singularity at a critical time t_c. Detailed descriptions of vortex methods and in particular the numerical difficulties associated with point-vortex methods are given by Meiron, Baker & Orszag (1982), Krasny (1986*a*), Rottman *et al.* (1987) and Rottman & Stansby (1993).

Of greatest relevance to the current study are the latter two papers, examining the evolution of a thin vortex sheet surrounding a cylinder of fluid released from rest in a

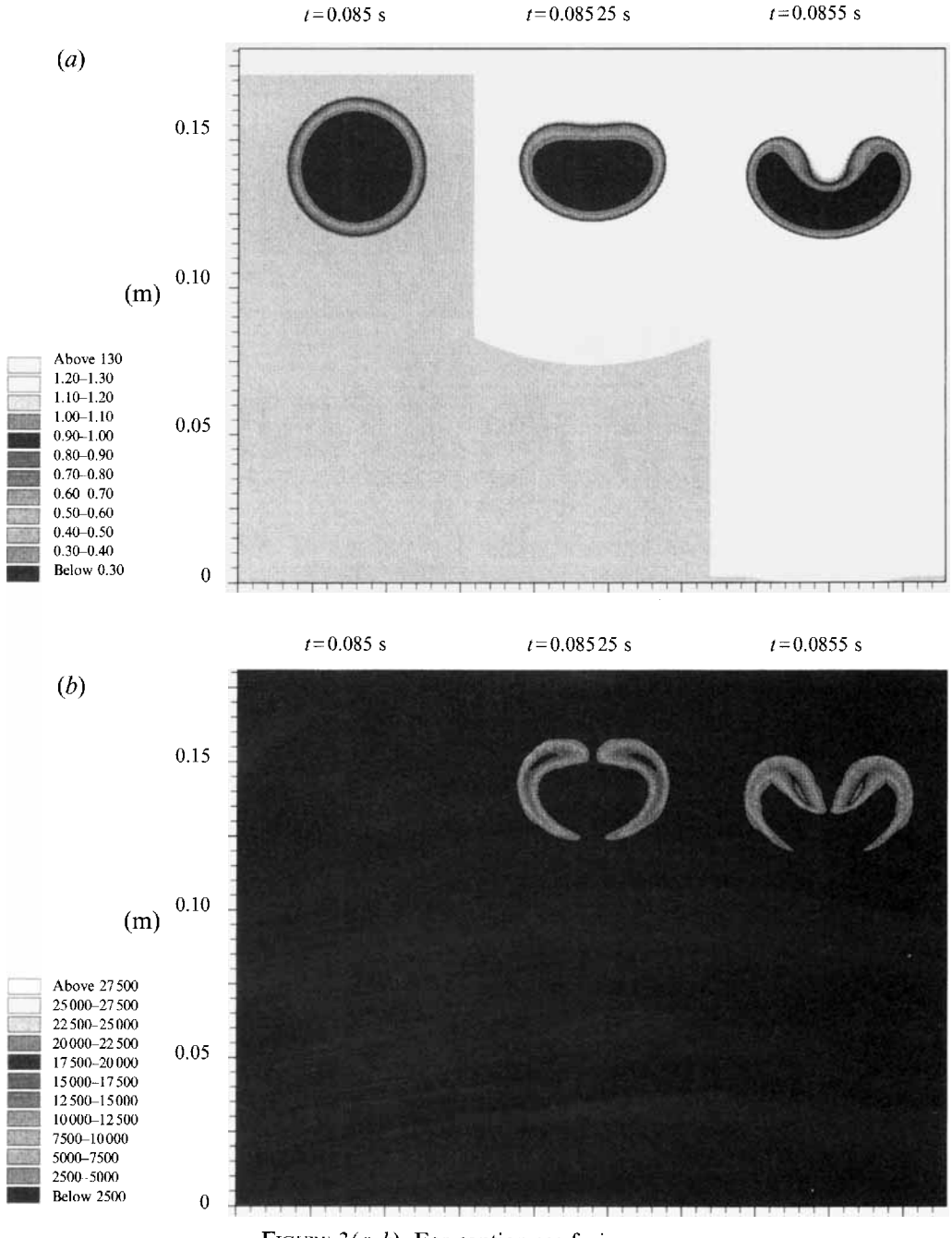

FIGURE 3(*a*, *b*). For caption see facing page.

cross-flow. Rottman *et al.* (1987) used the point-vortex method to derive solutions up to the critical time t_c for three different ratios of internal to external gas densities. In order to examine the continuing evolution of a cylindrical vortex sheet, Rottman & Stansby (1993) solve numerically the 'δ-equation', originally given by Krasny (1986*a*), which governs the evolution of vortex sheets embedded in a viscous incompressible

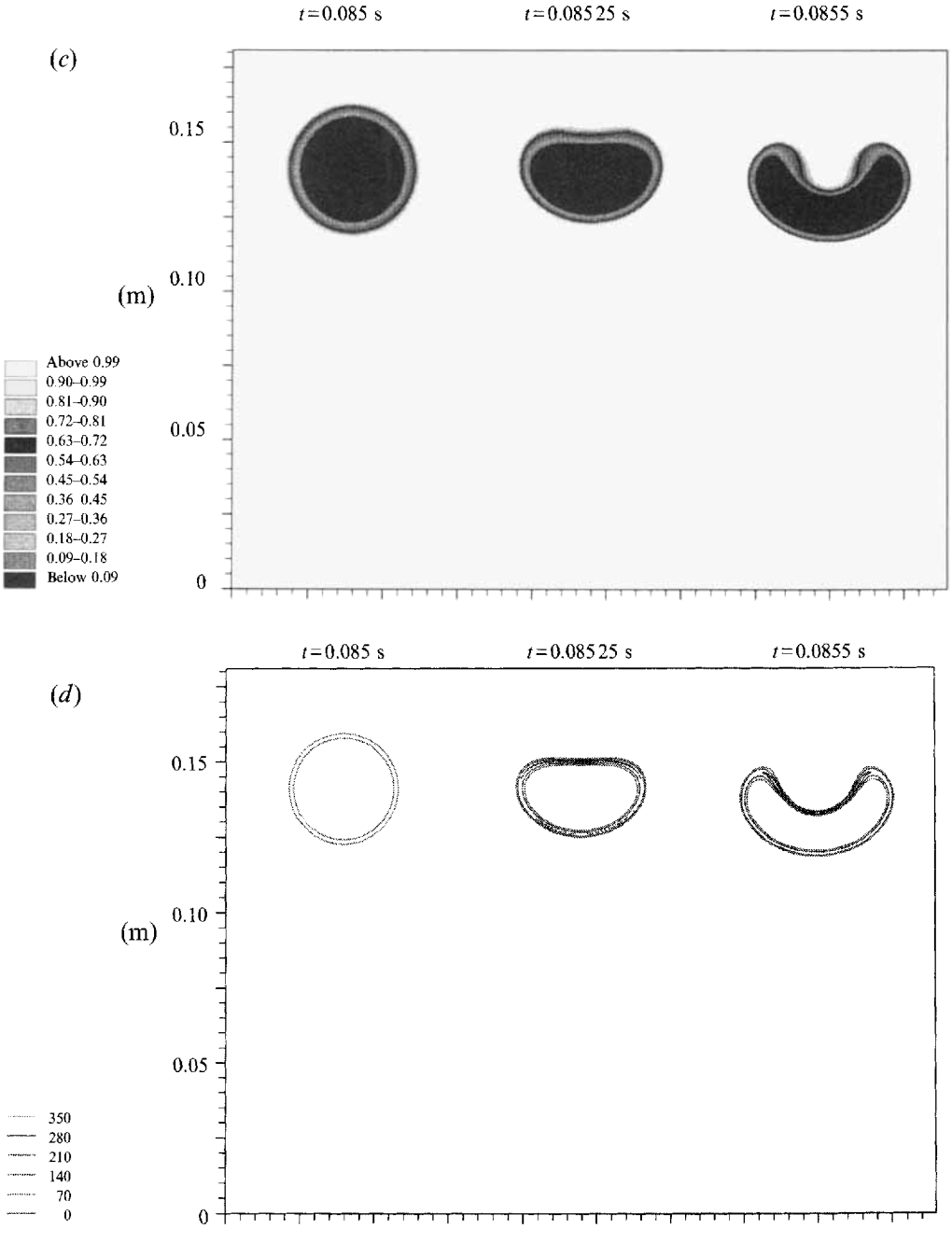

FIGURE 3. The initial evolution, generated by the interaction between a positive pressure step with fractional amplitude 0.3 and a cylindrical flame ball of radius 2 cm, of (*a*) the density distribution; (*b*) the vorticity field; (*c*) the fuel mass fraction distribution; and (*d*) the reaction rate distribution.

fluid whose density distribution is uniform. Thus they examine the evolution of a vortex sheet, whose locus is given in the complex plane by

$$z = r_0 \exp(\mathrm{i}\eta), \tag{6.3}$$

and whose vortex strength per unit azimuthal angle is given by

$$V(\eta) = -2U_0 r_0 \sin\eta. \tag{6.4}$$

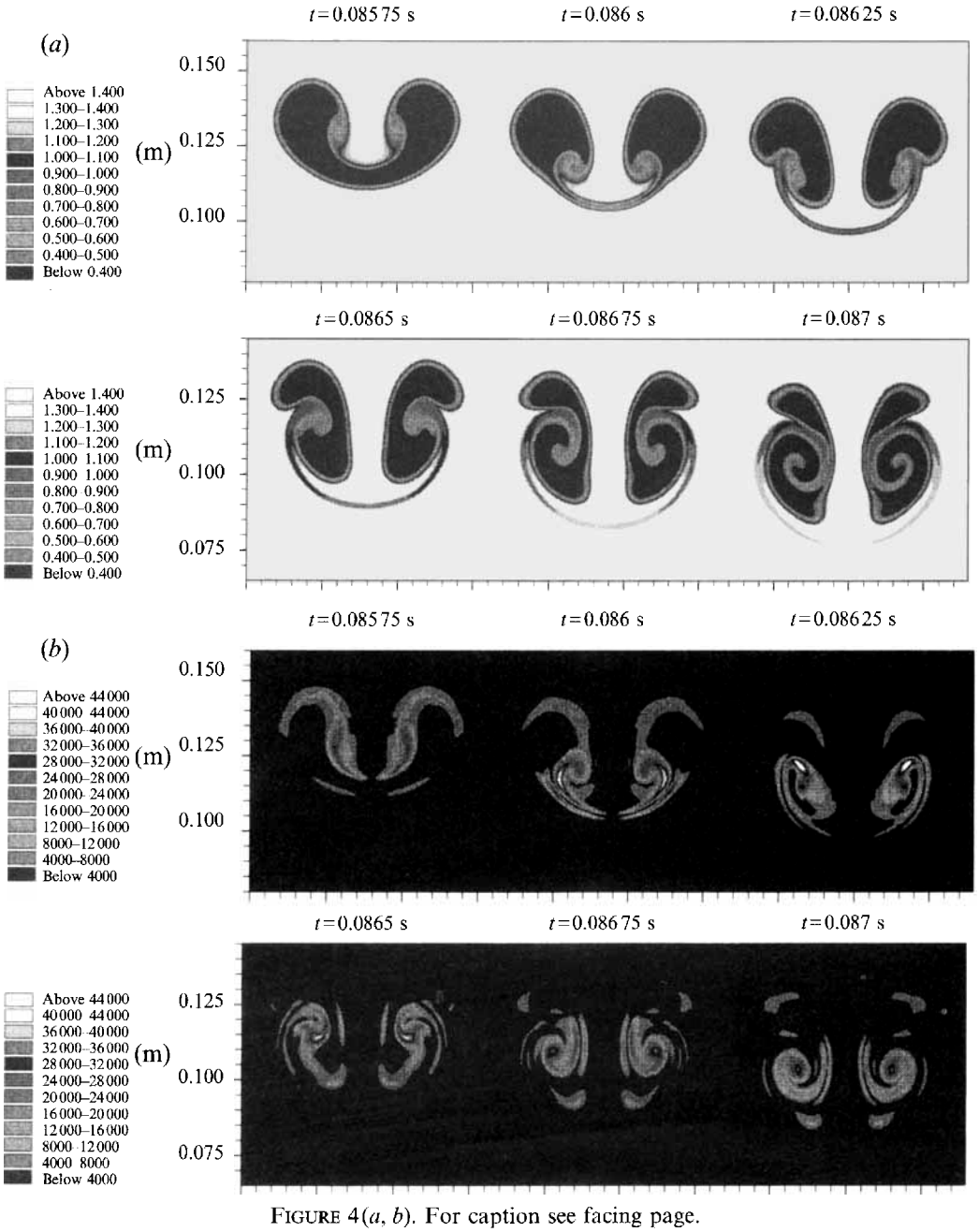

FIGURE 4(*a*, *b*). For caption see facing page.

Krasny's 'δ-equation' is given for a closed vortex sheet by

$$\frac{\partial z^*}{\partial t} = U_0 + \frac{1}{2\pi \mathrm{i}} \oint \frac{(z-z')^* V(\eta)\,\mathrm{d}z}{|z-z'|^2 + \delta^2}, \tag{6.5}$$

where the units of distance and time are given respectively by r_0 and r_0/U_0. Note that in these equations, the only effect of the U_0 term is a linear transformation of the vortex sheet, and so the important effects can be captured by setting this term to zero and

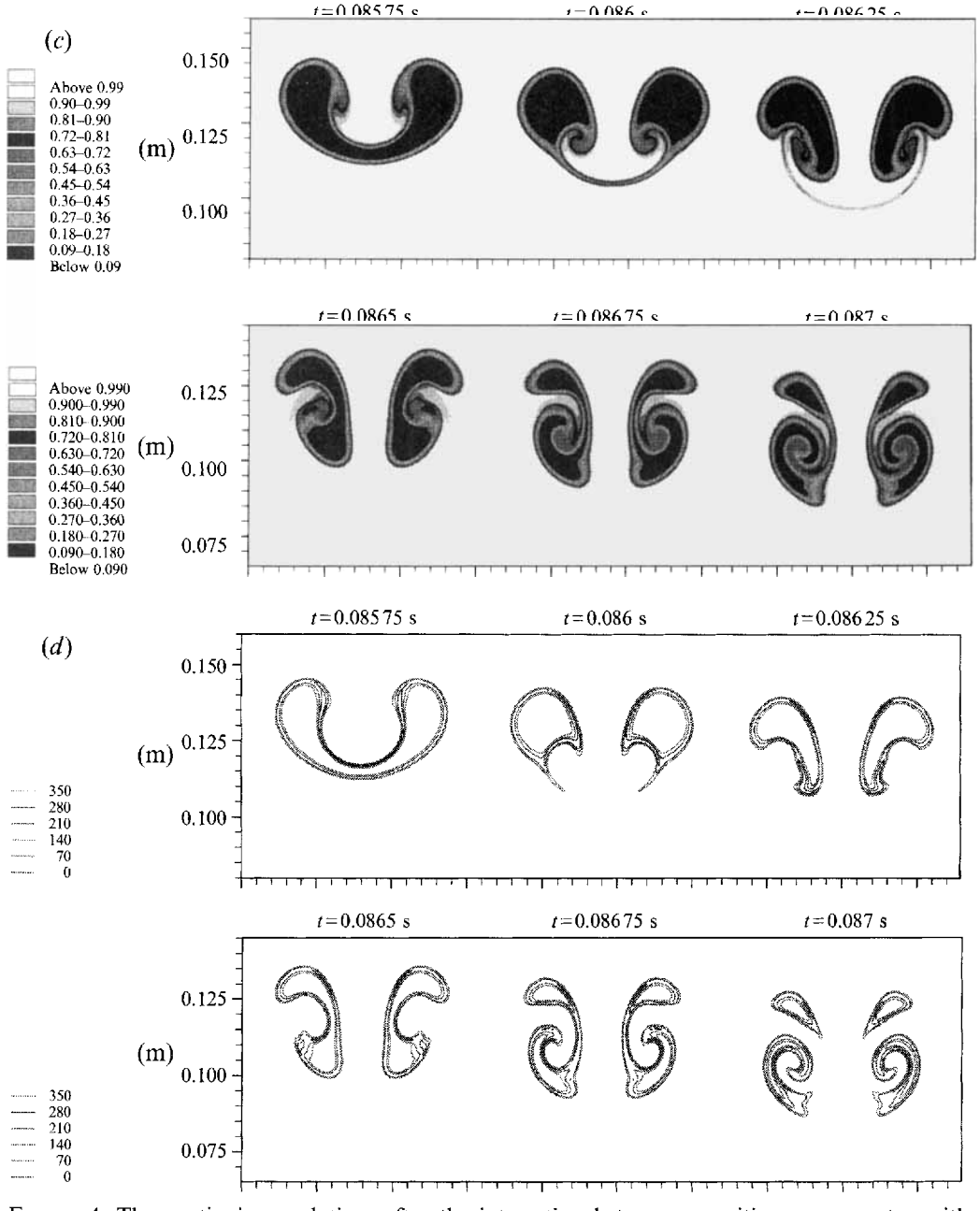

FIGURE 4. The continuing evolution, after the interaction between a positive pressure step with fractional amplitude 0.3 and a cylindrical flame ball of radius 2 cm, of (*a*) the density distribution; (*b*) the vorticity distribution; (*c*) the fuel-mass fraction distribution; and (*d*) the reaction rate distribution.

redefining the vortex-sheet strength separately. For the current set of parameters, equation (6.2) for the circulation strength per unit azimuthal angle gives

$$V(\eta) \approx -7 \sin \eta, \tag{6.6}$$

corresponding to $U_0 = 175$ m s^{-1}. (Here, $\eta = 0$ corresponds to the direction opposite to the initial direction of motion of the shock.) This then gives the equivalent length and time scales as 2 cm and 10^{-4} s. A non-zero value of δ is included in order to simulate

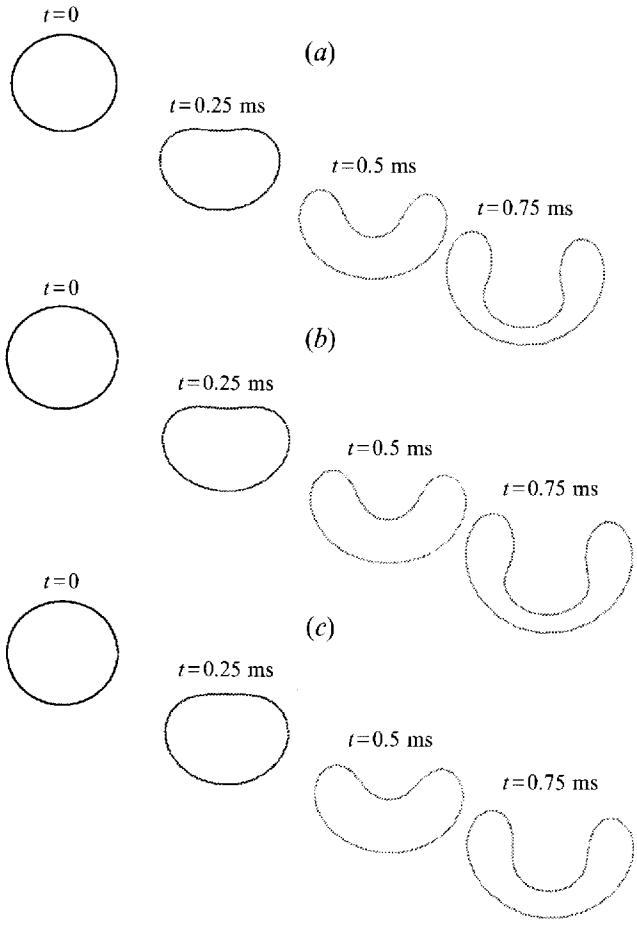

FIGURE 5. The evolution of a cylindrical vortex sheet released from rest at $t = 0$. ($N = 128$). (*a*) $\delta = 1.1$, (*b*) $\delta = 1.3$, (*c*) $\delta = 1.5$.

the effects of viscosity in resisting both the formation of a singularity at the critical time t_c, and the eventual rolling up of the vortex sheet into ever tighter coils. The amount of viscosity increases with the value of δ, and the overall effect is to decrease the rate of vortex-sheet roll-up. It is therefore likely that, although the results presented by Rottman *et al.* show much more rapid evolution than has been found in the numerical experiment described here, there exists an ideal value of δ for which the roll-up rate matches that found in this case. Of course, true comparisons will only be possible with the development of vortex methods to include the difference between the internal and external gas densities. However, it is worth considering what value of δ is required in the vortex-sheet formulation described in the above papers in order for the rate of roll-up to match the results of the direct numerical simulation described in the current paper. Figures 5(*a*)–5(*c*) show the results of numerical integrations of the vortex sheet 'δ-equations' (6.5). In each case, 128 data points are used, and as in the study by Krasny (1986*a*), a fast Fourier transform technique has been adopted in order to eliminate the 'saw-tooth' numerical instability described by that author. The results presented are for $\delta = 1.1$, $\delta = 1.3$, and $\delta = 1.5$ respectively. These values represent much higher viscosities than were used by Rottman *et al.* (1993), but it seems that a value in this range is required to give good qualitative agreement with the behaviour

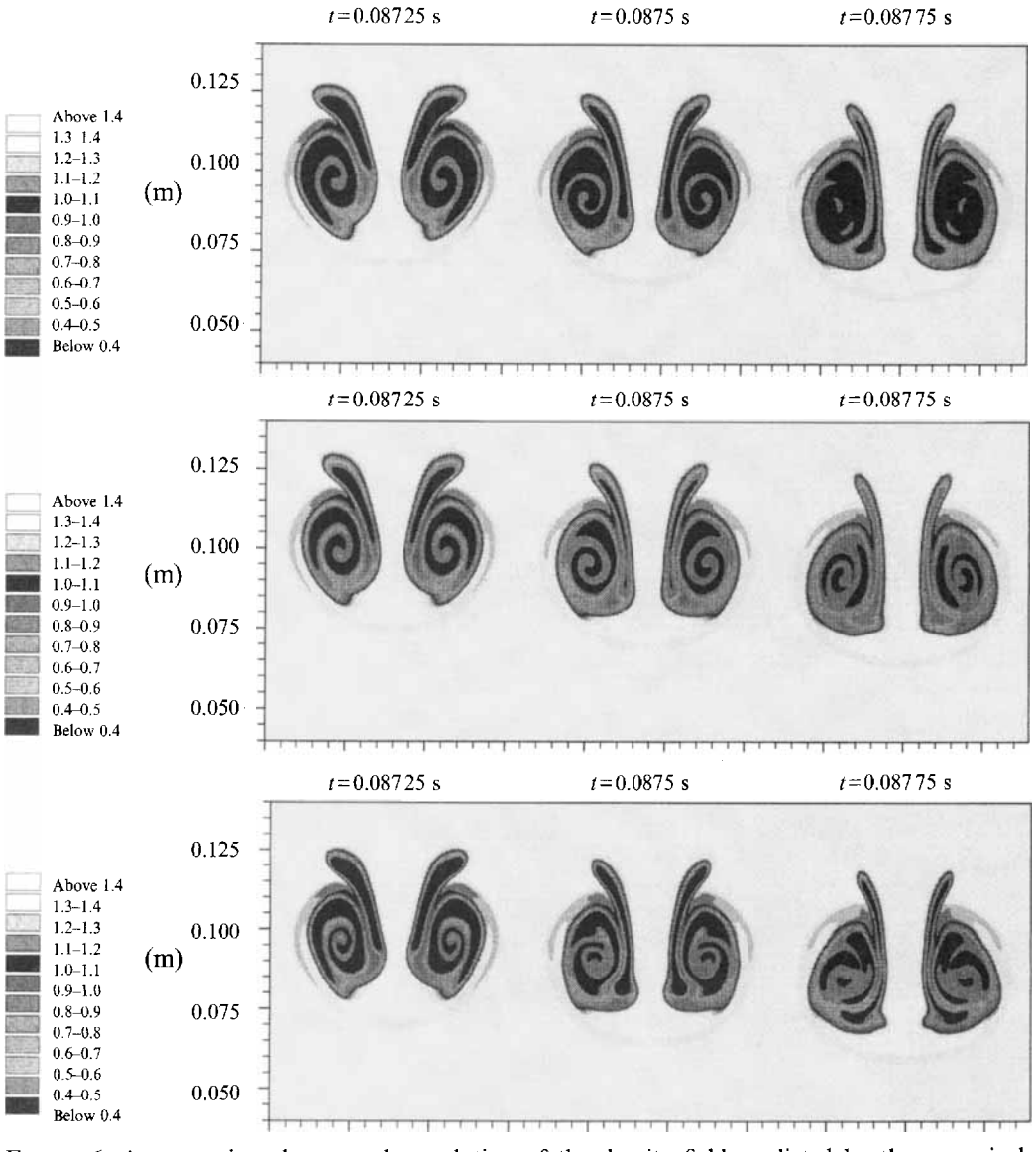

FIGURE 6. A comparison between the evolution of the density field predicted by the numerical solution of the full reactive–diffusive Navier–Stokes equations (top), the unreactive diffusive Navier–Stokes equations (middle) and the Euler equations (bottom).

of the flame (cf. figure 3(*a*) and the earliest time plot in figure 4*a*). Clearly, the vortex methods used here are incapable of predicting the behaviour of the flame with any rigour, since they have been developed to describe flows with uniform density. However, it has been shown here that it is possible to achieve approximate matching of the vortex-sheet roll-up timescale with that of the initial distortion of the flame front by choosing an appropriate value of the viscosity parameter δ.

6.2.2. *Effects of the reaction–diffusion system*

The results of the direct numerical simulation have clearly shown the creation of a strong vorticity field through the baroclinic effect caused by the of non-alignment of pressure and density gradients. In the previous section, comparisons with existing

vortex methods have shown qualitative agreement with the evolution of a cylindrical vortex sheet embedded in an ideal flow over early times. As described by the authors mentioned, the inclusion of viscous diffusion is crucial in obtaining meaningful results. Another important point of interest is the interaction between the vorticity field and the continuing evolution of the flame ball. The demonstration by Markstein (1964) that the double passage of a pressure signal across a flame ball could effect the transformation to turbulent burning clearly showed the importance of understanding the highly complex nonlinear interaction between vorticity fields and combustion systems. Although the experimental set-up modelled here involves only a single shock–flame interaction, and the reactivity of the mixture is very low (typified by a planar flame speed of less than 0.1 m s^{-1}), the reaction–diffusion processes do begin to affect the flow, even within a few milliseconds of the passage of the pressure disturbance across the flame. Figures 6 and 7 show comparisons between the continuing evolution of the flame ball under the influence of the baroclinically induced vorticity field (top), and the results of analogous numerical simulations of (i) an interaction between the same pressure signal and the same diffusive density distribution, with zero reaction rate (middle); and (ii) an interaction between the same pressure signal and the same initial density distribution with zero reaction rate and no diffusion (bottom).

As the numerical simulation proceeds, the cold unburnt gas from above is drawn right through the flame ball, splitting it into two separate components (see figure 6). within both components, each plot of figure 6 shows that the density distribution departs from the regular coil structure, although the reasons behind this part of the evolution are different in each of the three cases. The top three plots, showing the solution of the full equations, reveal the effect of the continuing chemical reaction. The unburnt gas drawn in from the exterior of the original flame ball is mixed with the hot burnt gas. As the cold gas is heated, it begins to burn, depositing more heat into the flow, which results in the tendency of the internal gas temperature to settle into a homogeneous distribution at around the adiabatic burnt gas temperature. This tendency is apparent in the rop right-hand plot of figure 6. In contrast, the solution of the unreactive Navier–Stokes equations (middle three plots of figure 6) shows that whilst the arms of the coil structure again tend to be thinned, because this is due to thermal and mass diffusion, the overall temperature of the gas is much lower (the density therefore being much higher).

It has been stated by previous authors such as Krasny (1968*a*, *b*) that an inviscid vortex sheet will always continue to roll up *ad infinitum*, so that numerical simulations which employ finite-difference methods will always reach a point where the results become heavily grid-dependent. This point appears to have been reached in the solution of the Euler equations shown in the bottom middle plot of figure 6, as the regular structure disintegrates to form a less ordered distribution. This is because there is no physical process included in that model whereby the continuing evolution into tighter and tighter coils can be resisted. As the two separate components continue to evolve, the point is therefore reached at which the grid becomes inadequate to capture accurately the sharpest gradients. Of course, if the grid size were to be reduced, this point would only be reached after a longer period of time, but as stated by previous authors such as Cloutman & Wehner (1992), this breakdown point is always reached in finite-difference Eulerian flow simulations which include significant vorticity fields.

Interesting effects are also revealed by the corresponding vorticity fields shown in figure 7. Again the solution of the Euler equations (bottom three plots) results in a somewhat disordered distribution by the time of the final (right-hand) plot.

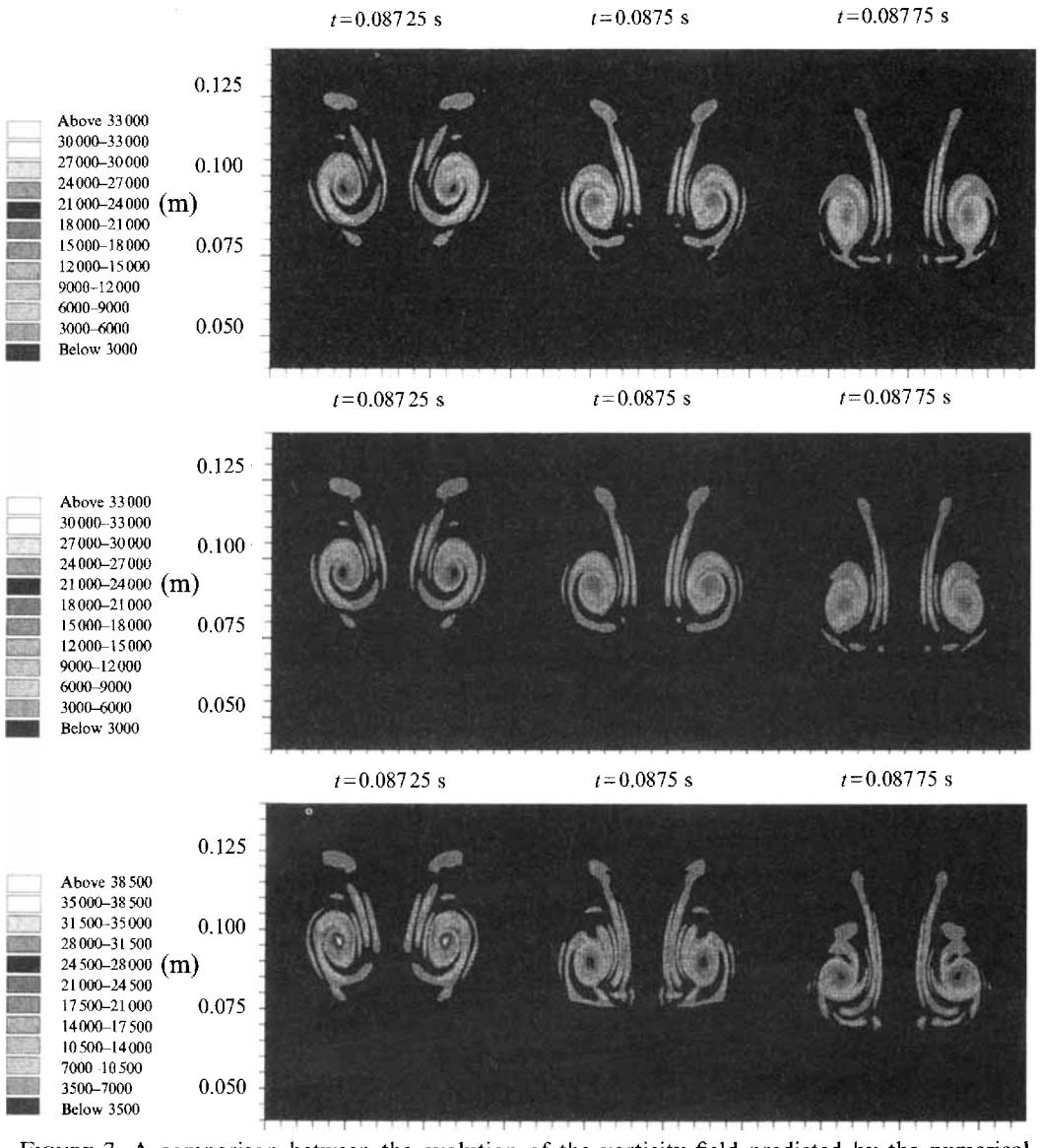

FIGURE 7. A comparison between the evolution of the vorticity field predicted by the numerical solution of the full reactive–diffusive Navier–Stokes equations (top), the unreactive diffusive Navier–Stokes equations (middle) and the Euler equations (bottom).

Comparison of the magnitude of the vorticity field reveals that the inclusion of diffusion processes reduces the magnitude of the final vorticity field, and that, when the chemical reaction is included, the vorticity field is further reduced. Clearly, dissipation of the vorticity field by viscous diffusion has been revealed. The extra reduction when the reaction term is included (note the higher vorticity values shown in the middle three plots compared with those in the top three plots) is due to the temperature dependence of the diffusion coefficients. (Without the chemical reaction, diffusive heat losses lead in turn to a reduction in the values of all of the diffusion coefficients.)

The continuing evolution of the two separate components requires further investigation. It seems likely that there are two possible eventual outcomes of this experiment. If the reaction rate is sufficiently rapid (after the adiabatic increase in

temperature associated with the incident pressure signal), it is likely that the two components will continue to evolve into rotating flame balls. It is possible, however, that if the intrusion of cold gas is too rapid, then the final temperature within each component may be too low for significant combustion to be maintained, and this swamping of the flame ball may cause extinction.

7. Concluding remarks

The plots of the two-dimensional interactions show that, for this relatively low reactivity, the initial evolution of the flame front is dominated by the Eulerian part of the governing equations, the chemical and thermal energies being convected with the evolving vorticity field, and the flame ball is split into two components by the intrusion of the cold gas through the central regions.

More meaningful modelling of this experiment using vortex methods clearly requires further development, including the development of a method to incorporate the propagation of the flame front during the roll-up of the vortex sheet. However, by choosing a very high value for the viscosity parameter δ, it has been possible to make qualitative comparisons between the behaviour of a vortex sheet and that of the annular vorticity field which is initially identified with the flame front, using vortex methods designed for uniform density fields. It would be interesting to investigate whether the same rough correspondence follows for pressure steps of any amplitude when the value of δ is kept constant and only the strength of the vortex sheet is changed.

The authors would like to thank the research groups of Dr G. O. Thomas of the Physics Department of Aberystwyth University as well as that of Dr C. Catlin at British Gas for useful discussions. The financial support for this work comes from the Science and Engineering Research Council and from British Gas.

REFERENCES

ANDERSON, C. 1985 A vortex method for flows with slight density variations. *J. Comp. Phys.* **61**, 417–444.

BATLEY, G. A. 1993 The interaction of pressure disturbances with premixed flames. PhD thesis, University of Leeds.

BATLEY, G. A., MCINTOSH, A. C. & BRINDLEY, J. 1993*a* The time evolution of interactions between short length scale pressure disturbances and premixed flames. *Combust. Sci. Tech.* **92**, 367–388.

BATLEY, G. A., MCINTOSH, A. C. & BRINDLEY, J. 1993*b* The evolution of premixed flame reaction zone structure under the influence of pressure fluctuations. *Proc. Joint Meeting of the British and German Sections of The Combustion Institute March/April 1993.* (ed. K. N. C. Bray *et al.*) pp. 311–314.

BOOK, D. L., BORIS, J. P., KUHL, A. L., ORAN, E. S., PICONE, J. M. & ZALESAK, S. T. 1981 Simulations of complex shock reflections from wedges in inert and reactive gas mixtures. In *Proc. Seventh Intl Conf. on Numerical Methods in Fluid Dynamics*, pp. 84–90.

CHORIN, A. J. & BERNARD, P. S. 1973 Discretization of a vortex sheet, with an example of roll-up. *J. Comput. Phys.* **13**, 423–429.

CLARKE, J. F. & MCINTOSH, A. C. 1984 Second order theory of unsteady burner-anchored flames with arbitrary Lewis number. *Combust. Sci. Tech.* **38**, 161–196.

CLOUTMAN, L. D. & WEHNER, M. F. 1992 Numerical simulation of Richtmeyer–Meshkov instabilities. *Phys. Fluids* A **4**, 1821–1830.

CRIGHTON, D. G. 1986 Basic theoretical nonlinear acoustics. *Frontiers in Physical Acoustics. Soc. Italiana di Fisica. XCIII Corso.*

FALLE, S. A. E. G. 1991 Self-similar jets. *Mon. Not. R. Astron. Soc.* **250**, 581–596.

KRASNY, R. 1986*a* A study of singularity formation in a vortex sheet by the point-vortex approximation. *J. Fluid Mech.* **167**, 65–93.

KRASNY, R. 1986*b* Desingularization of periodic vortex sheet roll-up. *J. Comput. Phys.* **65**, 292–313.

KRASNY, R. 1987 Computation of vortex sheet roll-up in the Trefftz plane. *J. Fluid Mech.* **184**, 123–155.

MARKSTEIN, G. H. 1964 Non-steady flame propagation. *AGAR Dograph* 75. Pergamon.

MCINTOSH, A. C. 1989 The interaction of high frequency low amplitude acoustic waves with premixed flames. In *Nonlinear Waves in Active Media* (ed. J. Engelbrecht), pp. 218–231. Springer.

MCINTOSH, A. C. 1991 Pressure disturbances of different lengthscales interacting with convcntional flames. *Combust. Sci. Tech.* **75**, 287–309.

MCINTOSH, A. C. 1993 The linearised response of the mass burning rate of a premixed flame to rapid pressure changes. *Combust. Sci. Tech.* **91**, 329–346.

MCINTOSH, A. C., BATLEY, G. A. & BRINDLEY, J. 1993 Short length scale pressure pulse interactions with premixed flames. *Combust. Sci. Tech.* **91**, 1–13.

MEIRON, D. I., BAKER, G. R. & ORSZAG, S. A. 1982 Analytic structure of vortex sheet dynamics. Part 1. Kelvin–Helmholtz instability. *J. Fluid Mech.* **114**, 283–298.

ORAN, E. S. & BORIS, J. P. 1979 Theoretical and computational approach to modeling flame ignition. *US Naval Research Rep., NRL Mem. Rep.* 4134.

PICONE, J. M., ORAN, E. S., BORIS, J. P. & YOUNG, T. R. 1984 Theory of Vorticity generation by shock wave and flame interactions. *Prog. Astronaut. Aeronaut., Dynamics of Shock Waves, Explosions and Detonations*, vol. 94, pp. 429–448.

ROTTMAN, J. W., SIMPSON, J. E. & STANSBY, P. K. 1987 The motion of a cylinder of fluid released from rest in a cross-flow. *J. Fluid Mech.* **177**, 307–337.

ROTTMAN, J. W. & STANSBY, P. K. 1993 On the 'δ-equations' for vortex sheet evolution. *J. Fluid Mech.* **247**, 527–549.

ROSENHEAD, L. 1931 The formation of vortices from a surface of discontinuity. *Proc. R. Soc. Lond.* A **134**, 170–192.

SCARINCI, T. 1990 The generation of vorticity by shock waves in a reactive flow. B. Engng thesis McGill University, Montreal, Canada.

SCARINCI, T. & THOMAS, G. O. 1992 Some experiments on shock-flame interaction. *University College of Wales, Aberystwyth Rep.* DET905.

TRYGGVASON, G., DAHM, W. J. A. & SBEITH, K. 1990 Fine structure of vortex sheet roll-up by viscous and inviscid simulation. *Trans. ASME* I: *J. Fluids Engng* **113**, 31–36.

WHITHAM, G. B. 1974 *Linear and Non-linear Waves*. Wiley.